EVALUATION OF THE USE OF GREEN LIQUOR DREGS IN THE PRODUCTION OF ALKALI-ACTIVATED MATERIALS

Oliveira, Cecilia Prado[1] and Motta, Leila Aparecida de Castro[2]
[1]Department of Civil Engineering, Federal University of Uberlândia, Uberlândia City, Brazil
ceciliaprado@ufu.br
[2] Department of Civil Engineering, Federal University of Uberlândia, Uberlândia City, Brazil
lacastro@ufu.br

ABSTRACT

The pulp and paper industry generates approximately 88 kg of solid waste per ton of paper produced. This paper investigates the use of green liquor dregs (GLD) from the kraft pulping stage to produce metakaolin-based alkali-activated binders. The residues were calcined at 915 °C for 2 h to generate reactive calcium oxide, considering its potential porosity-reducing effects on the pastes. The binder's properties were evaluated through an experimental design based on a central composite planning with three independent variables: the activator/precursor mass ratio; the curing time; and the content of thermally treated dregs as precursor. Spread, compressive strength, dynamic modulus of elasticity and drying shrinkage of the pastes were tested. It was observed that increasing activator/precursor mass ratio is detrimental to compressive strength, dynamic modulus of elasticity and drying shrinkage, due to excess sodium in the mixtures. The increase on percentage of GLD in the precursor also cause decrease on compressive strength and dynamic modulus of elasticity, which can be attributed to three main factors: a reduction of aluminosilicates available for alkali-activation; an insufficient amount of calcium oxide for C-A-S-H formation; and an increase on SiO_2/Al_2O_3 ratio lowering reaction speed. However, if associated with adequate activator/precursor ratio, the reduction in compressive strength is minimum, up to only 3.33 MPa. A decrease in the drying shrinkage of some pastes was also observed when increasing GLD content. These results demonstrate feasibility of the use of GLD in the production of alkali-activated binders.

KEYWORDS: *Alkali-activated Materials, Green Liquor Dregs, Thermal Treatment; Response Surface.*

I. INTRODUCTION

Alkali-activated binders are produced by a reaction between a source of aluminosilicate and an activating alkaline solution [1, 2]. These materials can reach elevated levels of mechanical strength and durability, in addition to dimensional stability, fire resistance and aggregate adherence [2–4]. These properties are influenced by many factors, such as calcium content, dosage and curing conditions [1].

The addition of reactive calcium oxide in alkali-activated binders produces a complex microstructure due to the formation of hydrated gels that can promote reduction in porosity and improvement in mechanical strength [5, 6].

The pulp and paper industry is characterized by its outstanding worldwide production. However, roughly 88 kg of solid waste are generated per ton of paper produced [7, 8]. Green liquor dregs (GLD) are generated during the chemical recovery stage in the kraft pulping process [9]. It is estimated that each ton of produced pulp generates 4 to 20 kg of GLD [10]. Although research has been done regarding GLD recycling [11 – 14], most of these residues are still dumped in landfills [15].

Research has been done on the use of GLD and other residues from the pulp and paper industry as fillers in the production of alkali-activated binders [15 – 19]. Studies regarding the activating effect of GLD have also been carried out [20 – 22]. However, there are no reports on the use of thermally treated GLD as a source of reactive calcium oxide in the mixtures.

This study aims to produce and characterize alkali-activated pastes with green liquor dregs generated from the pulp and paper industry, in order to investigate their mechanical properties and dimensional stability under drying shrinkage.

Following this introduction, this paper is structured into three sections. Section II, Materials and Methods, describes the materials used in the mixtures, the design of experiments, and the procedures employed during pastes preparation and characterization. Section III, Results and Discussion, presents response surfaces for each variable analysed, as well as a discussion of the results obtained, considering the published literature. Lastly, Section IV provides the conclusion of this study.

II. MATERIALS AND METHODS

2.1. Materials

The metakaolin used as the source of aluminosilicate in the mixtures was donated by Metacaulim do Brasil Indústria e Comércio Ltda., located in Jundiaí, Brazil. It was determined by X-ray fluorescence that the material is mainly composed of silicon dioxide (SiO_2 – 48.84%) and aluminium oxide (Al_2O_3 – 40.74%). The particle size distribution was obtained by laser diffraction, which showed a mean particle diameter of 18.25 μm.

The green liquor dregs were donated by Suzano S.A., located in Três Lagoas, Brazil. Its main mineral phase is calcite ($CaCO_3$), as identified by X-ray diffraction. The residues were oven-dried at 100 ºC for 24 h, milled and sieved. A mean particle size of 28.17 μm was obtained. The GLD were then thermally treated at 915 ºC for 2 h, as stablished at a previous work [23], in order to obtain reactive calcium oxide from the calcination of calcite.

The chemical analysis showed that thermally treated GLD are mainly composed of calcium oxide (CaO – 50.14%) and magnesium oxide (MgO – 16.67%). The presence of aluminosilicates (SiO_2 – 8.08%; Al_2O_3 – 2.79%) was also identified.

The activators consisted of a combination of a 15 M sodium hydroxide solution and a 12 M sodium silicate solution. Sodium hydroxide in flakes with a 96-99% purity was supplied by Start Química, and sodium silicate with a SiO_2/Na_2O mole ratio of 2 was supplied by Auro's Química Indústria e Comércio Ltda (SiO_2 = 52.8%; Na_2O = 25.8%; H_2O = 20.5%).

2.2. Design of Experiments (DOE)

In this work, the experiments were designed according to a central composite planning, which considered three independent variables: the activator/precursor mass ratio; the curing time; and the content of thermally treated dregs as precursor. Table 1 shows the coded and decoded values adopted for each variable. The alpha (α) coefficient of 1.682 was determined for rotatability. Four replicates at the central point were performed.

Table 1. Coded and uncoded levels of variables studied.

Variables	Symbol		Coded levels				
	Uncoded	Coded	–1.68	– 1	0	1	1.68
Activator/Precursor	A	x_1	0.5	0.54	0.6	0.66	0.7
Curing time (days)	CT	x_2	1	3	7	11	14
GLD (%)	D	x_3	0	4.05	10	15.95	20

The responses analysed were spread, compressive strength, dynamic modulus of elasticity and drying shrinkage of the pastes. The software Statistica® was used to conduct a regression analysis with a

significance level of 10% [24]. The response surface methodology was adopted for the evaluation of the effects of the independent variables on the responses.

2.3. Alkali-Activated Pastes Preparation

The activators were prepared with a mass ratio of 2.5 between sodium silicate and sodium hydroxide. The metakaolin and GLD were added to the mixture, along with water to ensure workability. The water/solid ratio was kept constant at 0.36 in all mixtures, which includes the amount of water used on the activating solutions.

After 5 minutes of mechanical mixing at 120 rpm, the pastes were poured in cubic molds (4 cm x 4 cm x 4 cm) for the compressive strength and dynamic modulus of elasticity tests. The mixtures were also casted into rectangular moulds, according to the sizes stablished at ABNT NBR 15261:2005, in order to determine the length change. The moulded samples were sealed and cured at 25 ± 5 ºC.

2.4. Characterization of the Pastes

2.4.1. Mini Slump

Mini slump tests were conducted according to the methods proposed by Kantro [25]. The pastes were poured into a truncated cone-shaped mould with an upper diameter of 2 cm, a lower diameter of 4 cm and a height of 6 cm. The mould was lifted, and the spread diameters were measured in two perpendicular directions after the flow was completed.

2.4.2. Compressive Strength Test

Compressive strength tests were performed on an Instron Universal Testing Machine, model 5982, at a load-applying speed of 500 N/s.

2.4.3. Dynamic Modulus of Elasticity

The dynamic modulus of elasticity of the pastes was determined by ultrasonic wave transmission, according to the methods proposed at ABNT NBR 8802:2019. The Ultrasonic Pulse Velocity Tester E48 by Controls was used to conduct the tests.

Transmitter and receiver transducers were fixed on opposite sides of the sample. Transmission time of the ultrasonic wave was measured, and dynamic modulus of elasticity was calculated through Equation (1).

$$E_d = v^2 \rho (1+\mu)(1-2\mu)/(1-\mu) \quad (1)$$

where E_d is dynamic modulus of elasticity, v is wave propagation velocity, ρ is apparent density, and μ is Poisson coefficient. A Poisson coefficient of 0.2 was adopted in the present work.

2.4.4. Length Change

The length change measurement was conducted in accordance with ABNT NBR 15261:2005. The samples were demoulded after 48 h, and the initial length was measured by a mechanical comparator with a 1 μm precision.

The pastes were cured at 25 ± 5 ºC and a relative humidity of 50 ± 8%. The length of the samples was measured at 1, 7, 14 and 28 days after demoulding.

2.4.5. Fourier Transform Infrared Spectroscopy (FTIR)

The specimens used to determine the length change were ground at 28 days and used as samples to perform Fourier transform infrared spectroscopy (FTIR).

IR measurements were conducted using a PerkinElmer Frontier spectrophotometer with an attenuated total reflection (ATR) module, scanning from 4000 cm^{-1} e 250 cm^{-1} with a 4 cm^{-1} resolution.

III. RESULTS AND DISCUSSION

3.1. Mini Slump

Equation (2) was obtained by multiple regression of the mini slump tests results in function of two independent variables: the activator/precursor mass ratio (x_1) and the percentage of thermally treated dregs in the precursor (x_3).

$$S. = 88.7 + 6.86x_1 - 3.35x_1^2 + 4.55x_3 - 0.97x_3^2 + 1.63x_1x_3 \quad (2)$$

where *S.* corresponds to the spread of the pastes in millimetres.

Table 2 shows the analysis of variance (ANOVA) for the quadratic model for spread. The linear and quadratic terms corresponding to the variable x_1 and the quadratic form of x_3 were significant, as well as their linear combination.

Table 2. Analysis of variance (ANOVA) for response surface quadratic model for spread (S.)

	Sum of squares	DF	Mean square	F value	Prob > F
x_1	642.620	1	642.620	101.2641	0.000
x_1^2	148.845	1	148.845	23.4550	0.000
x_3	283.342	1	283.342	44.6491	0.000
x_3^2	12.394	1	12.394	1.9530	0.188
x_1x_3	21.125	1	21.125	3.3289	0.093

The response surface, Figure 1, shows that spread increases with increasing activator/precursor mass ratio (x_1), which can be explained by an increase in pH and OH^- ions available for dissolution of the precursor [26, 27]. It can also be observed that spread increases with increasing percentage of thermally treated dregs in the precursor (x_3). This can be attributed to a higher mean particle diameter of GLD compared to metakaolin used in the mixtures, which reduces water demand and increases spread of the pastes [2, 28].

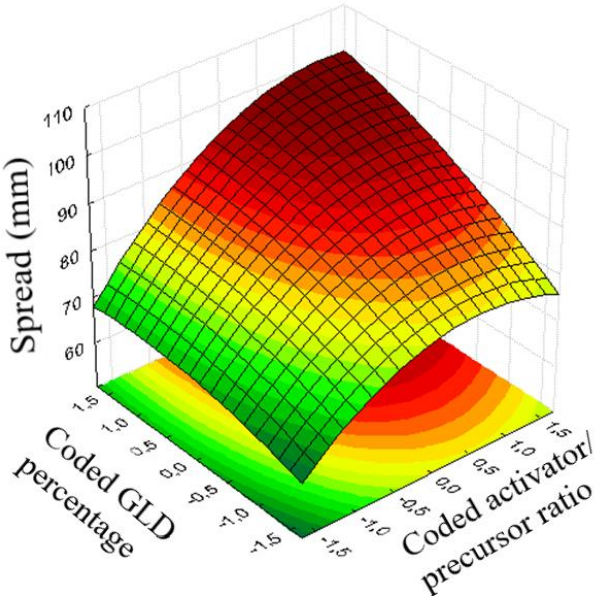

Fig. 1. Response surface of the spread (*S.*)

Optimization of the function was performed with the software Statistica®. A maximum point was identified at (x_1 = 2.00; x_3 = 4.06), corresponding to an activator/precursor mass ratio of 0.72 and 34.16% of GLD in the mixture. According to the statistical model, these values result in a spread of 104.74 mm.

3.2. Compressive Strength

Equation (3) represents the statistical model obtained by multiple regression of compressive strength of the alkali-activated pastes in function of: the activator/precursor mass ratio (x_1); the curing time (x_2); and the percentage of thermally treated dregs in the precursor (x_3).

$$C.S. = 26.65 - 2.4x_1 + 1.59x_1^2 + 4.59x_2 - 2.03x_2^2 - 2.01x_3 + 0.46x_3^2 - 1.14x_1x_2 + 0.24x_1x_3 + 0.31x_2x_3 \quad (3)$$

where *C.S.* is the compressive strength of the pastes in megapascal (MPa).

The ANOVA for the quadratic model for *C.S.*, Table 3, shows that the linear and quadratic terms corresponding to x_1 and x_2 and the linear term for x_3 were significant.

Table 3. Analysis of variance (ANOVA) for response surface quadratic model for compressive strength (C.S.)

	Sum of squares	DF	Mean square	F value	Prob > F
x_1	78.653	1	78.653	14.2295	0.005
x_1^2	32.009	1	32.009	5.7909	0.043
x_2	287.253	1	287.253	51.9683	0.000
x_2^2	52.002	1	52.002	9.4079	0.015
x_3	55.131	1	55.131	9.9740	0.013
x_3^2	2.733	1	2.733	0.4943	0.502
x_1x_3	10.323	1	10.323	1.8686	0.209
x_1x_2	0.447	1	0.447	0.0808	0.783
x_2x_3	0.750	1	0.750	0.1357	0.722

Figure 2 represents the response surface for compressive strength as a function of: activator/precursor mass ratio (x_1) and curing time (x_2) for GLD percentage (x_3) at a central level (Figure 2a); x_1 and x_3 for curing time at a central level (Figure 2b); and x_2 and x_3 for activator/precursor mass ratio at a central level (Figure 2c).

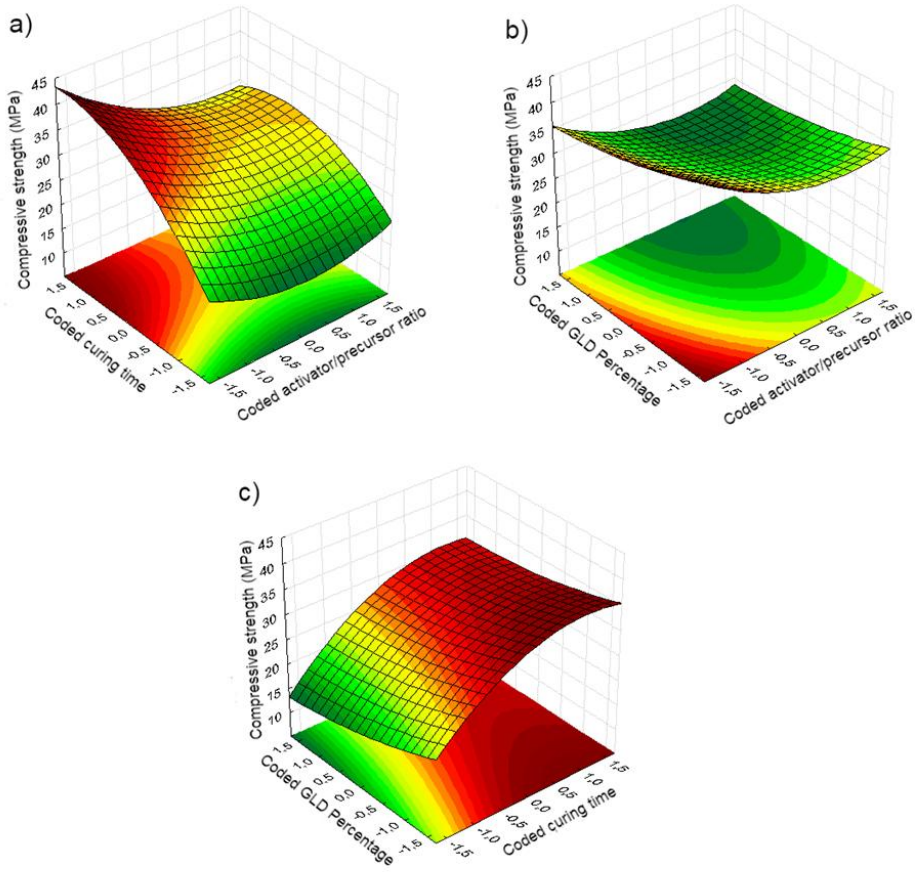

Fig. 2. Response surface of the compressive strength (*C.S.*): a) D at a central level ($x_3 = 0$); b) CT at a central level ($x_2 = 0$); c) A at a central level ($x_1 = 0$).

It was observed that compressive strength increases with curing time (x_2) due to the reorganization and development of the binder's microstructure [29]. On the other hand, *C.S.* decreases with increasing activator/precursor mass ratio (x_1). Although a higher activator concentration favors precursor's dissolution [30], excess sodium remains unbound and weakens the structure [31, 32].

Compressive strength also reduces due to the increment on percentage of thermally treated dregs in the precursor (x_3). This can be attributed to a decrease on aluminosilicates available for alkali-activation [33]. The amount of calcium oxide might also have been insufficient for C-A-S-H formation and refinement of the microstructure [5, 6]. In addition, GLD had a higher SiO_2/Al_2O_3 ratio than metakaolin used in the mixtures, which is often associated with a lower reaction speed [27, 34].

However, it should be noted that increasing GLD percentage in pastes with 0.54 and 0.66 activator/precursor mass ratio only caused minor reductions in compressive strength, of up to 3.33 MPa. Additionally, the highest strength achieved during the tests was 40.94 MPa at 7 days for the paste A0.5-D10, with 10% of dregs as precursor.

Optimization of the function showed a saddle point at ($x_1 = 0.99$; $x_2 = 0.98$; $x_3 = 1.59$), corresponding to a 0.659 activator/precursor ratio, 10.9 days of curing and 19.46% of GLD. This results in an estimated *C.S.* of 29.11 MPa.

3.3. Dynamic Modulus of Elasticity

Equation (4) was obtained by multiple regression of the dynamic modulus of elasticity of the binders as a function of activator/precursor mass ratio (x_1), curing time (x_2), and percentage of thermally treated GLD in the precursor (x_3).

$$M.E. = 11.15 - 0.39x_1 + 0.33x_1^2 + 0.44x_2 - 0.29x_2^2 - 0.38x_3 + 0.05x_3^2 - 0.05x_1x_2 - 0.02x_1x_3 + 0.14x_2x_3 \quad (4)$$

where *M.E.* corresponds to the dynamic modulus of elasticity of the pastes in gigapascal (GPa).

Table 4 shows the ANOVA for the quadratic model for *M.E.* The linear and quadratic terms for x_1 and the linear terms for x_2 and x_3 were significant.

Table 4. Analysis of variance (ANOVA) for response surface quadratic model for dynamic modulus of elasticity

	Sum of squares	DF	Mean square	F value	Prob > F
x_1	2.128	1	2.128	5.5076	0.047
x_1^2	1.345	1	1.345	3.4809	0.099
x_2	2.688	1	2.688	6.9571	0.030
x_2^2	1.057	1	1.057	2.7359	0.137
x_3	1.955	1	1.955	5.0608	0.055
x_3^2	0.034	1	0.034	0.0888	0.773
x_1x_3	0.020	1	0.020	0.0518	0.826
x_1x_2	0.002	1	0.002	0.0047	0.947
x_2x_3	0.151	1	0.151	0.3915	0.549

The response surfaces for the dynamic modulus of elasticity of the binders were plotted as a function of: x_1 and x_2 for GLD percentage at a central level (Figure 3a); x_1 and x_3 for curing time at a central level (Figure 3b); and x_2 and x_3 for activator/precursor mass ratio at a central level (Figure 3c).

Dynamic modulus of elasticity is related to an instantaneous strain, which depends on the microstructure and porosity of the pastes [35]. Therefore, the surfaces represented on Figure 3 exhibit a similar behavior to the compressive strength. *M.E.* increases with increasing curing time (x_2) and decreases with increasing activator/precursor mass ratio (x_1) and dregs percentage (x_3). It is believed that the reasons for these responses are the same as the ones discussed in Section 3.2.

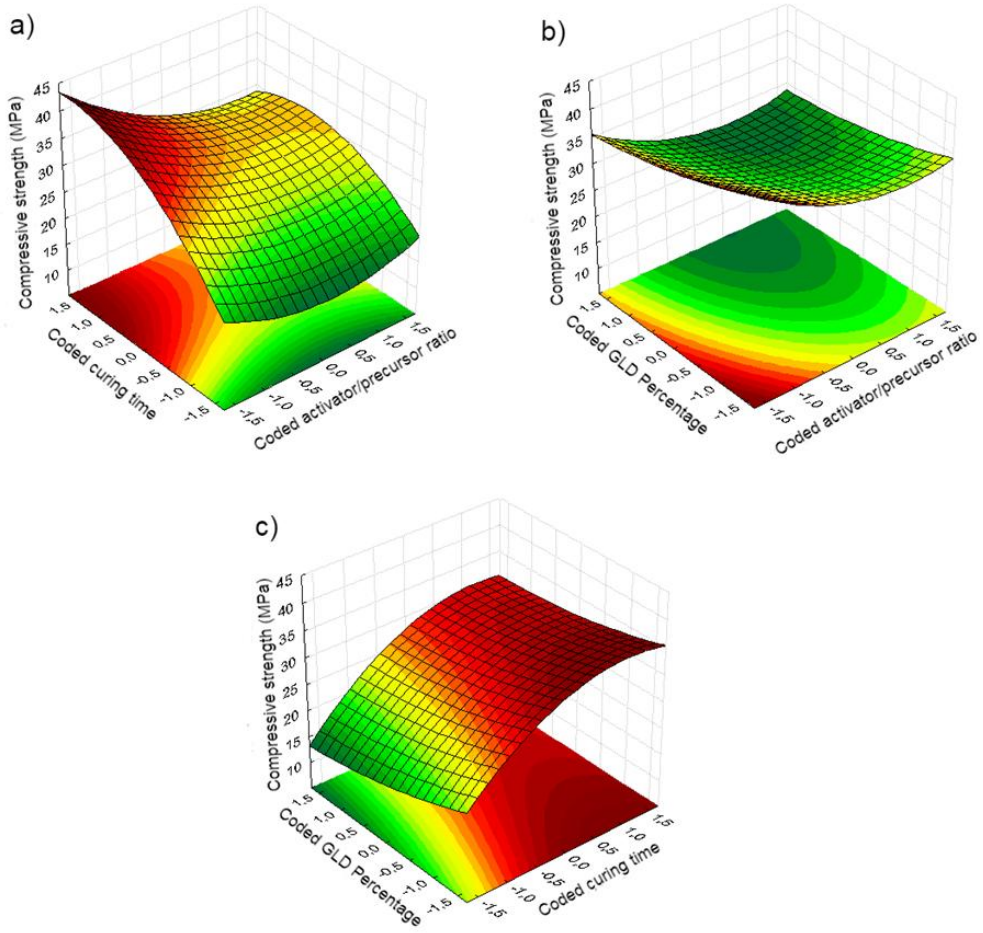

Fig. 3. Response surface of the dynamic modulus of elasticity (*M.E.*): a) D at a central level ($x_3 = 0$); b) CT at a central level ($x_2 = 0$); c) A at a central level ($x_1 = 0$).

By the optimization of the function, a saddle point was identified at ($x_1 = 0.75$; $x_2 = 1.21$; $x_3 = 2.14$). This corresponds to a 0.645 activator/precursor ratio, 2.16 days of curing and 22.73% of thermally treated dregs on the precursor, resulting in an estimated dynamic modulus of elasticity of 10.87 GPa.

3.4. Length Change

The samples used on the determination of length change showed different degrees of cracking related to the drying shrinkage. [36] reported a similar behavior on ground granulated blast furnace slag (GGBFS) based binders cured on air-dry environment.

Alkali-activated pastes with activator/precursor mass ratio of 0.5 and 0.54 had no signs of cracking, whereas samples with ratios of 0.7 and 0.66 exhibited substantial cracking. The length measurements of the pastes A0.66-D4.05, A0.7-D10 e A0.66-D15.95 were hindered by the degree of cracking 1, 7 and 14 days after demoulding, respectively.

Figure 4 shows the length change of the pastes as a function of time. It can be noted that drying shrinkage increases with increasing activator/precursor mass ratio, as reported by other authors [37, 38]. The compressive strength and dynamic modulus of elasticity results suggest that increasing activator concentration leads to a higher porosity in the microstructure. This reduces water evaporation restriction, which intensifies drying shrinkage [39].

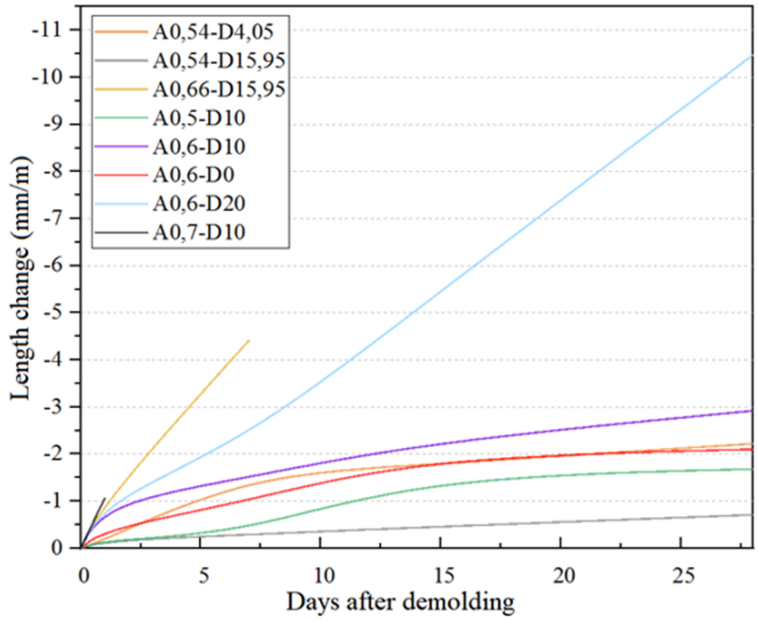

Fig. 4. Length change of the pastes as a function of time.

It was also observed that increasing GLD percentage decreased shrinkage in pastes with activator/precursor mass ratios of 0.54 and 0.66. The presence of magnesium oxide in GLD might have led to the formation of expansive phases, such as hydrotalcite and magnesium hydroxide, resulting in the reduction in shrinkage in those pastes [33, 36; 40 – 42]. However, this effect was not observed in mixtures with a 0.6 activator/precursor ratio, which can be attributed to significant water evaporation hindering the formation of shrinkage-reducing phases [39]. Nonetheless, it is noteworthy that water evaporation can be reduced by curing methods such as steam and water bath [36].

3.5. Fourier Transform Infrared Spectroscopy (FTIR)

Figure 5 shows the FTIR spectra of the pastes, which exhibited similar patterns for all mixtures.

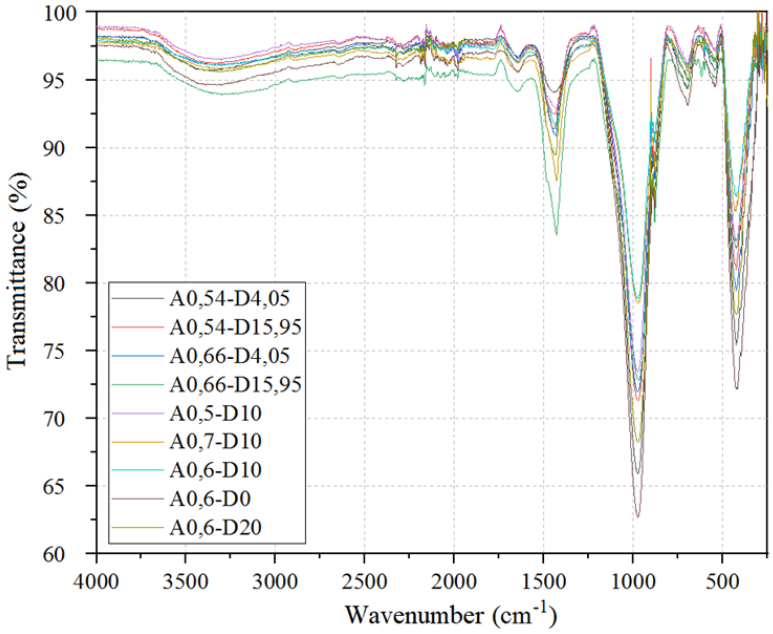

Fig. 5. FTR spectra of the pastes.

Table 5 summarizes the bands identified in the spectra. The bands from 3600 to 2950 cm^{-1} and the peak at 1645 cm^{-1} are related to the stretching and folding vibrations of the O–H. This can be attributed to the presence of imprisoned water in the microstructure [43, 44], but it can also indicate the presence of chemically bound water due to the formation of C-A-S-H and C-S-H gels [45, 46].

Table 5. Bands identified in the FTIR spectra

Wavenumber (cm^{-1})	Assignment
3600-2950	O–H stretching vibrations
1645	O–H folding vibrations
1430	C–O stretching vibrations
970	Si–O–Si and Si–O–Al stretching vibrations
700	Al–O–Si folding vibrations
545	Si–O folding vibrations
420	Al–O–Al folding vibrations

The peak close to 1430 cm^{-1} relates to the stretching vibration of C–O bonds. This indicates the presence of CO_3^{2-} due to the carbonatation of excess NaOH [46, 47]. The intensity of this peak increased with increasing the activator/precursor mass ratio in the pastes, owing to a higher amount of excess sodium in the mixture. This can explain the decrease in compressive strength and dynamic modulus of elasticity, as the carbonatation weakens the microstructure. It was also observed that the peak referring to C–O stretching vibrations increased with increasing GLD percentage. This can be explained by the higher porosity of these pastes facilitating CO_2 penetration [47].

The most intense peak in the FTIR spectra was identified at approximately 970 cm^{-1}. This band is associated with the stretching vibrations of Si–O–Si and Si–O–Al bonds, suggesting the formation of the N-A-S-H gel structure [44 – 48]. The tetrahedra SiO_4 in C-A-S-H and C-S-H gels can also contribute to the presence of this band [49 – 51]. It was observed that the intensity of this peak decreased with increasing GLD percentage, except for the mixture A0.6-D20. This behavior can be attributed to the reduction of aluminosilicates available for alkali-activation, as well as the reaction of Al–O and Si–O with MgO present in the residues to form hydrotalcite and magnesium silicate hydrate [33].

IV. CONCLUSIONS

The pulp and paper industry generates roughly 88 kg of solid waste per ton of paper produced, most of which is dumped in landfills.

This paper investigated the use of green liquor dregs from the kraft pulping process in the production of metakaolin-based alkali-activated binders. The residues were calcined at 915 ºC for 2 h to obtain reactive calcium oxide.

The spread of the binders showed a noticeable increase as the activator/precursor mass ratio was raised. This phenomenon can be attributed to the rise in pH and concentration of OH^- ions, facilitating the dissolution of the precursor material. Additionally, the spread of the binders also demonstrated an upward trend with increasing GLD percentage. This behavior can be linked to the larger mean particle size of GLD when compared to the metakaolin used in this study.

The compressive strength and dynamic modulus of elasticity of the pastes decreased with increasing activator/precursor mass ratio due to excess sodium remaining unbound in the mixtures. This suggests an increase in porosity, which explains the increment in drying shrinkage observed in the pastes with higher activator concentrations. Additionally, FTIR spectra indicates the presence C–O bonds, associated with carbonatation of excess sodium in the binders.

The compressive strength and dynamic modulus of elasticity increased with curing time, as expected based on the reorganization and development of the gel's microstructure. These properties decreased with increasing GLD percentage, which can be attributed to three main reasons: a reduction of

aluminosilicates available for alkali-activation; an insufficient amount of calcium oxide for C-A-S-H formation; and an increase on SiO_2/Al_2O_3 ratio, which is often associated with a lower reaction speed.

Nevertheless, it is noteworthy that increasing GLD percentage in pastes with activator/precursor mass ratio of 0.54 and 0.66 caused a small reduction in compressive strength, up to only 3.33 MPa. These pastes also showed a reduction in drying shrinkage with increasing GLD content, which can be explained by the formation of expansive phases, such as hydrotalcite and magnesium hydroxide, due to the presence of MgO in the residues. Besides, the highest strength achieved in the tests was 40.94 MPa at 7 days, corresponding to the mixture A0.5-D10. This shows that the use of green liquor dregs to produce alkali-activated binders is attainable when associated with an optimal activator/precursor ratio.

ACKNOWLEDGEMENTS

The authors would like to acknowledge Metacaulim do Brasil Indústria e Comércio Ltda. and Suzano S.A. for the donations of metakaolin and green liquor dregs.

REFERENCES

[1]. Provis, J.L. & Bernal, S.A. (2014) Geopolymers and related alkali-activated materials. *Annual Review of Materials Research.* Vol. 44., Pp. 299-327.

[2]. Duxson, P., Fernández-Jiménez, A., Provis, J.L., Lukey, G.C., Palomo, A. & Van Deventer, J.S.J. (2007) Geopolymer technology: the current state of the art. *Journal of Materials Science.* Vol. 42, No. 9, Pp. 2917-2933.

[3]. Juenger, M.C.G., Winnefeld, F., Provis, J.L. & Ideker, J.H. (2011) Advances in alternative cementitious binders. *Cem. and Conc. Res.* Vol. 41., Pp. 1232-1243.

[4]. Sujitha, V.S., Raja, S., Rusho, M.A., Yishak, S. (2025) Advances and developments in high strength geopolymer concrete for sustainable construction – A review. *Case Studies in Construction Materials.* Vol. 22, Pp. e04669.

[5]. Provis, J.L., Myers, R.J., White, C.E., Rose, V. & Van Deventer, J.S. (2012) X-ray microtomography shows pore structure and tortuosity in alkali-activated binders. *Cement and Concrete Research.* Vol. 42, No. 6, Pp. 855-864.

[6]. Yip, C.K. & Van Deventer, J.S.J. (2003) Microanalysis of calcium silicate hydrate gel formed within a geopolymeric binder. *Journal of Materials Science.* Vol. 38, No. 18. Pp. 3851-3860.

[7]. Zhang, Q., Khan, M.U., Lin, X., Yi, W. & Lei, H. (2020) Green-composites produced from waste residue in pulp and paper industry: A sustainable way to manage industrial wastes. *Journal of Cleaner Production.* Vol. 262., Pp. 121251.

[8]. Haile, A., Gelebo, G.G., Tesfaye, T., Mengie, W., Mebrate, M.A., Abuhay, A. & Limeneh, D.Y. (2021) Pulp and paper mill wastes: utilizations and prospects for high value-added biomaterials. *Bioresources and Bioprocessing.* Vol. 8, No. 1, Pp. 1-22.

[9]. Quina, M.J. & Pinheiro, C.T. (2020) Inorganic waste generated in kraft pulp mills: the transition from landfill to industrial applications. *Applied Sciences.* Vol. 10, No. 7, Pp. 2317.

[10]. Nurmesniemi, H., Pöykiö, R., Perämäki, P. & Kuokkanen, T. (2005) The use of a sequential leaching procedure for heavy metal fractionation in green liquor dregs from a causticizing process at a pulp mill. *Chemosphere.* Vol. 61, No. 10, Pp. 1475-1484.

[11]. Mäkelä, M.; Harju-Oksanen, M.L., Watkins, G., Ekroos, A. & Dahl, O. (2012) Feasibility assessment of inter-industry solid residue utilization for soil amendment—trace element availability and legislative issues. *Resources, Conservation and Recycling.* Vol. 67, Pp. 1-8.

[12]. Miranda, L.D.A., Alvarenga, R.D.C.S.S.A., Pinto, P.C.M., Júnior, E.D.D., Carvalho, C.A.B.D., Fassoni, D.P. & Couto, L.G. (2011) Avaliação do potencial do grits como material de construção na produção de tijolos de solo-cimento. *Revista Árvore.* Vol. 35, No. 6, Pp. 1335-1340.

[13]. Martínez-Lage, I.; Velay-Lizancos, M., Vázquez-Burgo, P., Rivas-Fernández, M., Vázquez-Herrero, C., Ramírez-Rodríguez, A. & Martín-Cano, M. (2016) Concretes and mortars with waste paper industry: biomass ash and dregs. *Journal of Environmental Management.* Vol. 181, Pp. 863-873.

[14]. Shavalieva, G., Olivegren, H., Baumann, H., Leventaki, E., Couto Queiroz, E., & Bernin, D. (2025). Green liquor dregs for carbon capture, utilization, and storage: initial LCA and economic analysis. *Nordic Pulp & Paper Research Journal*, No. 0.

[15]. Novais, R.M., Carvalheiras, J., Senff, L., Seabra, M.P., Pullar, R.C. & Labrincha, J.A. (2019) In-depth investigation of the long-term strength and leaching behaviour of inorganic polymer mortars containing green liquor dregs. *Journal of Cleaner Production.* Vol. 220., Pp. 630-641.

[16]. Novais, R.M., Carvalheiras, J., Senff, L. & Labrincha, J. A. (2018) Upcycling unexplored dregs and biomass fly ash from the paper and pulp industry in the production of eco-friendly geopolymer mortars: A preliminary assessment. *Construction and Building Materials.* Vol. 184., Pp. 464-472.

[17]. La Scalia, G., Saeli, M., Adelfio, L. & Micale, R. (2021) From lab to industry: Scaling up green geopolymeric mortars manufacturing towards circular economy. *Journal of Cleaner Production.* Vol. 316, Pp. 128164.

[18]. Saeli, M., Micale, R., Seabra, M.P., Labrincha, J.A. & La Scalia, G. (2020) Selection of novel geopolymeric mortars for sustainable construction applications using fuzzy topsis approach. *Sustainability.* Vol. 12, No. 15, Pp. 5987.

[19]. Siqueira, L. V. M. (2024). *Geopolímero com adição de dregs como alternativa de material de reparo em estruturas de cimento Portland* (Doctoral dissertation, Universidade do Estado de Santa Catarina).

[20]. Rasmus, J., Ohenoja, K., Kinnunen, P., & Illikainen, M. (2023). Effect of green liquor dregs as an alkali source for alkali-activated blast furnace slag mortar. *Case Studies in Construction Materials*, Vol. 18, Pp. e01950.

[21]. Rasmus, J., Adesanya, E., & Kilpimaa, K. (2024). Utilization of pretreated green liquor dregs as an activator for blast furnace slag: Effect on hydration, phase assemblage, and rheology. *Journal of Environmental Management*, Vol. 370, Pp. 123021.

[22]. Rasmus, J. (2025). Utilization of pulp mill side streams as a part of cementitious binders.

[23]. Oliveira, C.P. & Motta, L.A.C. (2022) Tratamento térmico de resíduos dregs para a produção de ligantes álcali-ativados. *Proceedings of International Congress of Civil Construction.* Brasília, 2022. Pp. 367-375.

[24]. Santos, M.A., Santana, R.C., Capponi, F., Ataíde, C.H. & Barrozo, M.A. (2010) Effect of ionic species on the performance of apatite flotation. *Separation and Purification Technology.* Vol. 76, No. 1, Pp. 15-20.

[25]. Liu, G., Cheng, W., Chen, L., Pan, G. & Liu, Z. (2020) Rheological properties of fresh concrete and its application on shotcrete. *Construction and Building Materials.* Vol. 243, Pp. 118180.

[26]. Dörr, G., Gasperi, J., Sattler, N.S. & Martínez, E.D.R. (2020) Mini-slump: aplicação de ensaio tradicional para avaliação da trabalhabilidade em estado fresco de geopolímeros à base de metacaulim. *Proceedings of 9th Internacional Forum Ecoinovar.* Santa Maria, 2020.

[27]. Yun-Ming, L.Y., Cheng-Yong, H., Al Bakri M.M. & Hussin, K. (2016) Structure and properties of clay-based geopolymer cements: a review. *Progress in Materials Science.* Vol. 83, Pp. 595-629.

[28]. Li, C., Sun, H. & Li, L. (2010) A review: the comparison between alkali-activated slag (Si + Ca) and metakaolin (Si + Al) cements. *Cement and Concrete Research.* Vol. 40, No. 9, Pp. 1341-1349.

[29]. Tashima, M.M., Soriano, L., Borrachero, M.V., Monzó, J. & Payá, J. (2013) Effect of curing time on microstructure and mechanical strength development of alkali activated binders based on vitreous calcium aluminosilicate (VCAS). *Bulletin of Materials Science.* Vol. 36, No. 2, Pp. 245-249.

[30]. Shi, X., Zha, Q., Li, S., Cai, G., Wu, D. & Zhai, C. (2022) Experimental study on the mechanical properties and microstructure of metakaolin-based geopolymer modified clay. *Molecules.* Vol. 27, No. 15, Pp. 4805.

[31]. Lancellotti, I., Catauro, M., Ponzoni, C., Bollino, F. & Leonelli, C. (2013) Inorganic polymers from alkali activation of metakaolin: effect of setting and curing on structure. *Journal of Solid-State Chemistry.* Vol. 200, Pp. 341-348.

[32]. Granizo, M.L., Blanco-Varela, M.T. & Martínez-Ramírez, S. (2007) Alkali activation of metakaolins: parameters affecting mechanical, structural and microstructural properties. *Journal of Materials Science.* Vol. 42, No. 9, Pp. 2934-2943.

[33]. Abdel-Gawwad, H.A. & El-Aleem, S. (2015) Effect of reactive magnesium oxide on properties of alkali activated slag geopolymer cement pastes. *Ceramics–Silikáty.* Vol. 59, No. 1, Pp. 37-47.

[34]. Provis, J.L. & Van Deventer. (2007) Direct measurement of the kinetics of geopolymerisation by in-situ energy dispersive x-ray diffractometry. *Journal of Materials Science.* Vol. 42, No. 90, Pp. 2974-2981.

[35]. Mehta, P.K. & Monteiro, P.J.M. (2006) *Concrete: microstructure, properties and materials,* 3rd ed., McGraw-Hill Publishing.

[36]. Chen, Y.C., Lee, W.H., Cheng, T.W., Chen, W. & Li, Y.F. (2022) The length change ratio of ground granulated blast furnace slag-based geopolymer blended with magnesium oxide cured in various environments. *Polymers.* Vol. 14, No. 16, Pp. 3386.

[37]. Zhan, J., Li, H., Pan, Q., Cheng, Z., Li, H. & Fu, B. (2022) Effect of slag on the strength and shrinkage properties of metakaolin-based geopolymers. *Materials.* Vol. 15, No. 8, Pp. 2944.

[38]. Fu, B., Cheng, Z., Han, J. & Li, N. (2021) Understanding the role of metakaolin towards mitigating the shrinkage behavior of alkali-activated slag. *Materials.* Vol. 14, No. 22, Pp. 6962.

[39]. Yang, T., Zhu, H. & Zhang, Z. (2017) Influence of fly ash on the pore structure and shrinkage characteristics of metakaolin-based geopolymer pastes and mortars. *Construction and Building Materials.* Vol. 153, Pp. 284-293.

[40]. Li, Z., Zhang, W., Wang, R., Chen, F. & Jia, X., Cong, P. (2019) Effects of reactive mgo on the reaction process of geopolymer. *Materials.* Vol. 12, No. 3, Pp. 526.

[41]. Yang, Y., Chen, Z., Feng, W., Nong, Y., Yao, M. & Tang, Y. (2021) Shrinkage compensation design and mechanism of geopolymer pastes. *Construction and Building Materials.* Vol. 299, Pp. 123916.

[42]. Shen, W., Wang, Y., Zhang, T., Zhou, M., Li, J. & Cui, X. (2011) Magnesia modification of alkali-activated slag fly ash cement. *Journal of Wuhan University of Technology-Mater.* Vol. 26, No. 1, Pp. 121-125.

[43]. Lin, K.L., Shiu, H.S., Shie, J.L., Cheng, T.W. & Hwang, C.L. (2012) Effect of composition on characteristics of thin film transistor liquid crystal display (TFT-LCD) waste glass-metakaolin-based geopolymers. *Construction and Building Materials.* Vol. 36, Pp. 501-507.

[44]. Belmokhtar, N., Ammari, M., Brigui, J. & Allal, L.B. (2017) Comparison of the microstructure and the compressive strength of two geopolymers derived from metakaolin and an industrial sludge. *Construction and Building Materials.* Vol. 146, Pp. 621-629.

[45]. Kapeluszna, E., Kotwica, L., Różycka, A. & Gołek, L. (2017) Incorporation of al in CASH gels with various Ca/Si and Al/Si ratio: microstructural and structural characteristics with DTA/TG, XRD, FTIR and TEM analysis. *Construction and Building Materials.* Vol. 155, Pp. 643-653.

[46]. Silveira, N.C.G., Martins, M.L.F., Da Silva Bezerra, A.C. & Da Silva Araújo, F.G. (2022) Ecological geopolymer produced with a ternary system of red mud, glass waste, and Portland cement. *Cleaner Engineering and Technology.* Vol. 6, Pp. 100379.

[47]. Aouan, B., Alehyen, S., Fadil, M., Alouani, M.E., Khabbazi, A., Atbir, A. & Taibi, M.H. (2021) Compressive strength optimization of metakaolin-based geopolymer by central composite design. *Chemical Data Collections.* Vol. 31, Pp. 100636.

[48]. Rożek, P., Król, M. & Mozgawa, W. (2018) Spectroscopic studies of fly ash-based geopolymers. *Spectrochimica Acta Part A: Molecular and Biomolecular Spectroscopy.* Vol. 198, Pp. 283-289.

[49]. Bernal, S.A., de Gutierrez, R.M., Provis, J.L. & Rose, V. (2010) Effect of silicate modulus and metakaolin incorporation on the carbonation of alkali silicate-activated slags. *Cement and Concrete Research.* Vol. 40, No. 6, Pp. 898-907.

[50]. Chindaprasirt, P. & Somna, K. (2015) Effect of addition of microsilica and nanoalumina on compressive strength and products of high calcium fly ash geopolymer with low concentration NaOH. *Advanced Materials Research.* Vol. 1103, Pp. 29-36.

[51]. Puertas, F., Palacios, M., Manzano, H., Dolado, J.S., Rico, A. & Rodríguez, J. (2011) A model for the cash gel formed in alkali-activated slag cements. *Journal of the European Ceramic Society.* Vol. 31, No. 12, Pp. 2043-2056.

AUTHORS

Cecilia Prado de Oliveira holds a B.Sc. in Civil Engineering from ESAMC Uberlândia (2018) and an M.Sc. in Civil Engineering from the Federal University of Uberlândia (2023). She is currently pursuing her Ph.D. in Civil Engineering at the Federal University of Uberlândia. Her professional background includes experience in civil construction and sanitation. Her research focuses on construction materials, particularly the development of alternative binders derived from waste materials.

Leila Aparecida de Castro Motta holds a B.Sc. in Civil Engineering from the Federal University of Uberlândia (1994), an M.Sc. in Structural Engineering from the University of São Paulo – São Carlos School of Engineering (1997), and a Ph.D. from the Polytechnic School of the University of São Paulo (2006). She is currently an Associate Professor at the Federal University of Uberlândia. Her research focuses on Civil Construction, with an emphasis on construction materials and components, particularly the use of natural plant fibers for reinforcement in cementitious and polymeric composites, as well as the incorporation of waste materials for the development of new and/or modified construction materials.